Vector Control of Double-Delta Sourced Winding for a Dual-Winding Induction Machine

Yongsoon Park, *Member, IEEE*, Jeong-Mock Yoo, and Seung-Ki Sul, *Fellow, IEEE*

***Abstract*—Ripple currents can be mitigated in motor drives by applying double-delta sourced winding (DDSW), which uses a multilevel operation approach with two-level converters. In practice, a dual-winding induction machine (DWIM) has been considered for this application due to its inherent compatibility with DDSW. The modeling of a DDSW-based DWIM is discussed for vector control, and a decoupling method between converters is proposed to improve the dynamic response of the current regulation. In addition, torque control is discussed for a situation in which one of the converters is dropped out. The effectiveness of the proposed methods is assessed via experiments under low switching frequencies because DDSW is appropriate for high-power applications, where multiple windings are essential. It was confirmed that the total harmonic distortion of the converter currents was decreased by 67.7% when an 11-kW DWIM was driven on the basis of DDSW. Furthermore, the bandwidth of the current regulation could be increased by 113.7% owing to the proposed decoupling method.**

***Index Terms*—Double delta, fault, induction machine, multilevel, vector control.**

I. Introduction

THE double-delta sourced transformer (DDST) was proposed to mitigate ripple currents through multilevel operations [1]. This topology is based on the fact that multiple windings are essential for power sharing in high-power systems [2]–[4]. In particular, induction machines are mainly used in large-scale industrial drives and are broadly classified according to their starting methods [5]–[7]. One type uses a series winding connection for starting and a parallel winding connection for normal operation. The induction machine for this starting method is known as a dual-winding induction machine (DWIM) and is deemed an appropriate candidate for use with double-delta sourced winding (DDSW).

A vector control scheme should be discussed for a DWIM because it is essential for high-performance drives [8]–[10]. The conventional modeling of DWIM may be helpful for vector control in DDSW schemes [11], [12]. However, the stator windings of induction machines are generally assumed to be wye connected in the literature, whereas they must be delta connected in DDSW schemes. Hence, by considering the delta connection, the electrical modeling of a DWIM is newly derived with respect to converter currents as opposed to winding currents. Accordingly, torque, flux, and slip equations are detailed for vector control of the DWIM for which DDSW is applied.

In addition, decoupling control between converters should be discussed with regard to current regulation. That is, every winding in DDSW is simultaneously affected by both converters. Although this can lead to better harmonic properties in combination with interleaving [1], [13], it increases the design complexity with reference to the current regulation when compared to cases in which dual-stator windings are separately driven [14]. For simple implementation and better dynamics, it is desirable to minimize any voltage/current couplings in the current regulation. In this paper, a novel decoupling method is proposed for which the voltage equation of a DDSW-based DWIM is rewritten.

Meanwhile, in DDSW, if one of the converters is dropped out for any reason, it would be desirable to continuously keep the other converter working. If one converter cannot operate due to a fault, it is isolated from the system by the opening of breakers [15]. Thus, under this form of single-converter operation, different modeling should also be derived for vector control. Even if the remaining converter solely deals with the series windings, it can operate with an identical dc-link voltage under its normal current limit. The harmonic property of the currents under this form of single-converter operation is shown as well.

All of the proposed methods are evaluated with a small-scale induction machine, which is a commercial product designed for dual-voltage sources, specifically 220/440 V. In the experimental results, the characteristics of DDSW are clearly confirmed at winding voltages and converter currents. It is also assessed whether the torque is regulated as intended through the vector control scheme. In addition, the effects of the decoupling method are discussed when torque references vary in a stepwise manner.

II. Double-Delta Sourced Winding

In Fig. 1(a), electrical connections are shown when DDSW is applied to motor drives. For simplicity, the magnetic coupling between the rotor and stator windings is depicted as a rotary transformer [16]. The influence of converters can be better understood when only the stator windings are considered, as shown in Fig. 1(b) [1]. In this figure, the three-phase outputs from two converters are connected to the "abc" and "rst" nodes, and the pairs of windings with identical back

Manuscript received February 19, 2016; revised May 17, 2016 and July 20, 2016; accepted July 30, 2016. Date of publication August 30, 2016; date of current version January 18, 2017. Paper 2016-IDC-0184.R2, presented at the 2015 9th International Conference on Power Electronics and ECCE Asia, Seoul, South Korea, June 1–5, and approved for publication in the IEEE TRANSACTIONS ON INDUSTRY APPLICATIONS by the Industrial Drives Committee of the IEEE Industry Applications Society.

Y. Park is with the Gwangju Institute of Science and Technology, Gwangju 61005, South Korea (e-mail: yongsoon@gist.ac.kr).

J.-M. Yoo is with the Yura Corporation R&D Center, Seongnam-si 463-742, South Korea (e-mail: jeongmock@eepel.snu.ac.kr).

S.-K. Sul is with the Seoul National University, Seoul 151-742, South Korea (e-mail: sulsk@plaza.snu.ac.kr).

Color versions of one or more of the figures in this paper are available online at http://ieeexplore.ieee.org.

Digital Object Identifier 10.1109/TIA.2016.2604313

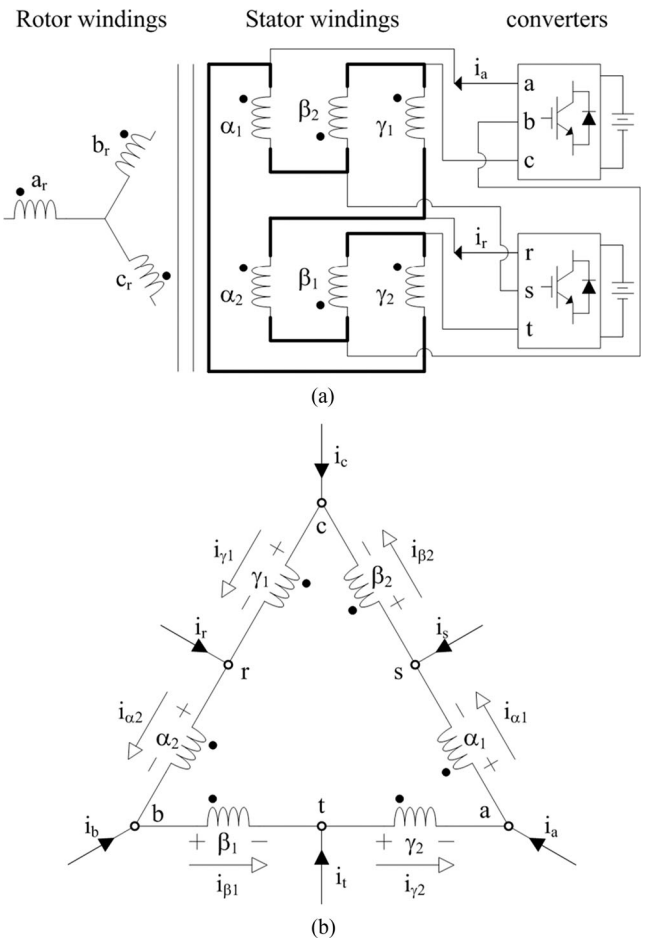

Fig. 1. Circuit diagrams when DDSW is applied to motor drives: (a) Motor and converters connection and (b) stator windings only.

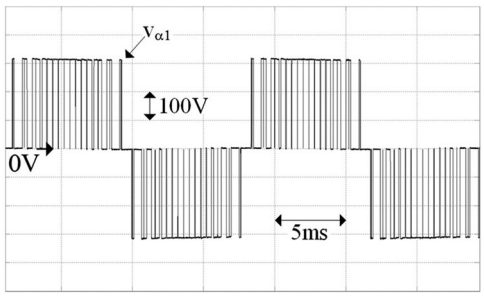

Fig. 2. Winding voltage in the conventional structure.

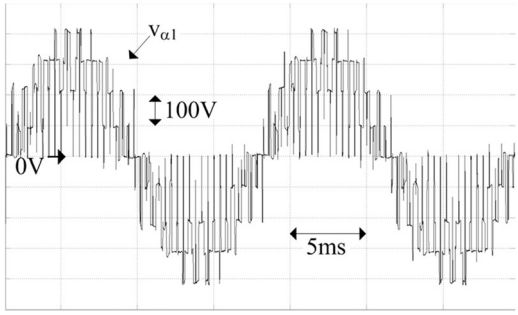

Fig. 3. Winding voltage in DDSW.

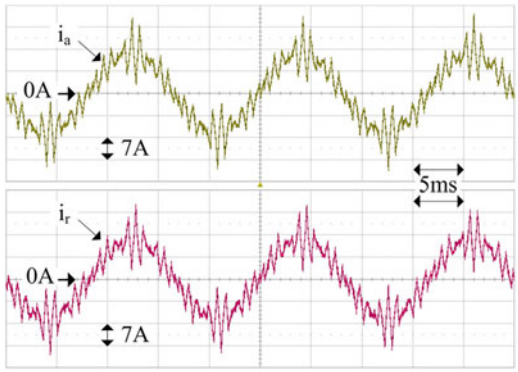

Fig. 4. Converter currents in the conventional structure.

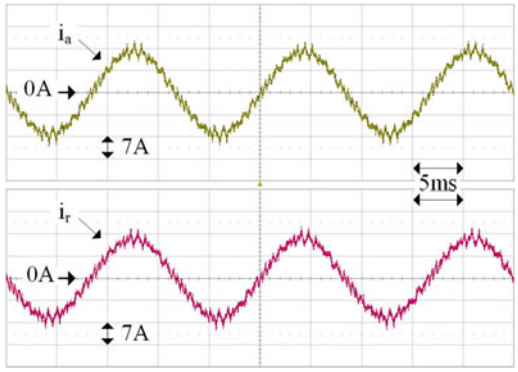

Fig. 5. Converter currents in DDSW.

electromotive forces (EMFs) are separated by the Greek letters "$\alpha\beta\gamma$." Thus, it can be inferred that each winding is affected by both of the converters. In other words, the pulse width modulation (PWM) of one converter affects all of the winding voltages simultaneously. Therefore, the harmonic distortions of the winding currents could be improved by appropriately adjusting the PWM combination for both converters.

The effect of DDSW can be clearly demonstrated by comparing the voltage and current of the conventional structures, shown in Figs. 2 and 4 with those in Figs. 3 and 5. Hereafter, the conventional structure refers to the case where each three-phase delta winding is galvanically isolated when driving [1]. In addition, the phase difference between the PWM carriers of each converter was set to 180° for both the conventional structure and DDSW.

At first, the winding voltages of α_1 (see Fig. 1) are shown in Figs. 2 and 3 according to the winding structures when an 11-kW DWIM is driven with no load at the rated speed. By comparing the figures, it is easily recognized that the voltage level is increased by DDSW, as in the case of DDST [1]. The property of the winding voltages is reflected directly into the converter currents, as shown in Figs. 4 and 5. While the fundamental currents are around 12.6 A for both figures, the total

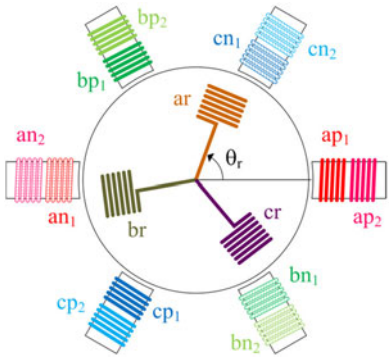

Fig. 6. Conceptual winding structure of a two-pole DWIM for DDSW.

harmonic distortion (THD) of the current is decreased by 67.7%, from 31.5% to 10.2%, by means of DDSW. When considering DDST [1], even if the interleaving effect is nearly identical on the rotor side for both the conventional structure and DDSW, it is very different on the stator side. This improvement on the stator side originates from the different winding structure and can contribute to higher conversion efficiency by mitigating the harmonics.

The back EMFs induced on α_1, β_1, and γ_1 are ideally expected to be identical to those on α_2, β_2, and γ_2, respectively. In other words, two sets of the three-phase windings are identical in terms of their influence on the rotating flux. The equivalent two-pole machine can, thus, be modeled for a DWIM, as shown in Fig. 6. Because this machine does not correspond to the case of a split phase belt [17], [18], the mutual coupling between the leakage inductances could be neglected.

III. Modeling of a DWIM for DDSW

Each winding of a DWIM has an identical voltage rating. Therefore, the rated voltage of a DWIM in a series connection would be twice that in parallel connection. For example, in Fig. 6, if the windings of $\mathrm{ap_1}$ and $\mathrm{ap_2}$ are series connected for 440 V, their parallel connection would be used for 220 V. That is, a commercial 220-/440-V DWIM can be used for DDSW.

The magnetic couplings among the stator and the rotor windings are derived as (1) by the principle described in the literature [8]

$$\begin{bmatrix}\lambda_{\alpha1}\\ \lambda_{\beta1}\\ \lambda_{\gamma1}\end{bmatrix} = \mathrm{L_{ls}}\begin{bmatrix}\mathrm{i}_{\alpha1}\\ \mathrm{i}_{\beta1}\\ \mathrm{i}_{\gamma1}\end{bmatrix} + \mathrm{L_{ms}A_m}\begin{bmatrix}\mathrm{i}_{\alpha1}+\mathrm{i}_{\alpha2}\\ \mathrm{i}_{\beta1}+\mathrm{i}_{\beta2}\\ \mathrm{i}_{\gamma1}+\mathrm{i}_{\gamma2}\end{bmatrix} + \mathrm{L_{ms}T_{rs}}\begin{bmatrix}\mathrm{i_{ar}}\\ \mathrm{i_{br}}\\ \mathrm{i_{cr}}\end{bmatrix} \tag{1-a}$$

$$\begin{bmatrix}\lambda_{\alpha2}\\ \lambda_{\beta2}\\ \lambda_{\gamma2}\end{bmatrix} = \mathrm{L_{ls}}\begin{bmatrix}\mathrm{i}_{\alpha2}\\ \mathrm{i}_{\beta2}\\ \mathrm{i}_{\gamma2}\end{bmatrix} + \mathrm{L_{ms}A_m}\begin{bmatrix}\mathrm{i}_{\alpha1}+\mathrm{i}_{\alpha2}\\ \mathrm{i}_{\beta1}+\mathrm{i}_{\beta2}\\ \mathrm{i}_{\gamma1}+\mathrm{i}_{\gamma2}\end{bmatrix} + \mathrm{L_{ms}T_{rs}}\begin{bmatrix}\mathrm{i_{ar}}\\ \mathrm{i_{br}}\\ \mathrm{i_{cr}}\end{bmatrix} \tag{1-b}$$

$$\begin{bmatrix}\lambda_{\mathrm{ar}}\\ \lambda_{\mathrm{br}}\\ \lambda_{\mathrm{cr}}\end{bmatrix} = (\mathrm{L_{lr}}+\mathrm{L_{ms}A_m})\begin{bmatrix}\mathrm{i_{ar}}\\ \mathrm{i_{br}}\\ \mathrm{i_{cr}}\end{bmatrix} + \mathrm{L_{ms}T_{sr}}\begin{bmatrix}\mathrm{i}_{\alpha1}+\mathrm{i}_{\alpha2}\\ \mathrm{i}_{\beta1}+\mathrm{i}_{\beta2}\\ \mathrm{i}_{\gamma1}+\mathrm{i}_{\gamma2}\end{bmatrix}. \tag{1-c}$$

Here, $\mathrm{L_{ls}}$ and $\mathrm{L_{lr}}$ are the leakage inductances of the stator and rotor windings, respectively. In addition, $\mathrm{L_{ms}}$ is the mutual inductance. The unexplained matrices in (1) are shown as

$$\mathrm{A_m} = \begin{bmatrix}1 & -1/2 & -1/2\\ -1/2 & 1 & -1/2\\ -1/2 & -1/2 & 1\end{bmatrix} \tag{2-a}$$

$$\mathrm{T_{rs}} = \begin{bmatrix}\cos\theta_\mathrm{r} & \cos\left(\theta_\mathrm{r}+\frac{2\pi}{3}\right) & \cos\left(\theta_\mathrm{r}-\frac{2\pi}{3}\right)\\ \cos\left(\theta_\mathrm{r}-\frac{2\pi}{3}\right) & \cos\theta_\mathrm{r} & \cos\left(\theta_\mathrm{r}+\frac{2\pi}{3}\right)\\ \cos\left(\theta_\mathrm{r}+\frac{2\pi}{3}\right) & \cos\left(\theta_\mathrm{r}-\frac{2\pi}{3}\right) & \cos\theta_\mathrm{r}\end{bmatrix} \tag{2-b}$$

$$\mathrm{T_{sr}} = \begin{bmatrix}\cos\theta_\mathrm{r} & \cos\left(\theta_\mathrm{r}-\frac{2\pi}{3}\right) & \cos\left(\theta_\mathrm{r}+\frac{2\pi}{3}\right)\\ \cos\left(\theta_\mathrm{r}+\frac{2\pi}{3}\right) & \cos\theta_\mathrm{r} & \cos\left(\theta_\mathrm{r}-\frac{2\pi}{3}\right)\\ \cos\left(\theta_\mathrm{r}-\frac{2\pi}{3}\right) & \cos\left(\theta_\mathrm{r}+\frac{2\pi}{3}\right) & \cos\theta_\mathrm{r}\end{bmatrix} \tag{2-c}$$

where θ_r is the rotor angle, which is defined in Fig. 6.

The flux equation in (1) pertains to the winding currents. However, it is more practical to consider the converter currents than the winding currents because current sensors for the current regulation are commonly installed in the converters. Equation (3) is derived from Fig. 1(b) by Kirchhoff's current law

$$\begin{cases}\mathrm{i_a} = \mathrm{i}_{\alpha1} - \mathrm{i}_{\gamma2}\\ \mathrm{i_b} = \mathrm{i}_{\beta1} - \mathrm{i}_{\alpha2}\\ \mathrm{i_c} = \mathrm{i}_{\gamma1} - \mathrm{i}_{\beta2}\end{cases} \tag{3-a}$$

$$\begin{cases}\mathrm{i_r} = \mathrm{i}_{\alpha2} - \mathrm{i}_{\gamma1}\\ \mathrm{i_s} = \mathrm{i}_{\beta2} - \mathrm{i}_{\alpha1}\\ \mathrm{i_t} = \mathrm{i}_{\gamma2} - \mathrm{i}_{\beta1}\end{cases}. \tag{3-b}$$

When considering (3), (1) can be rearranged into the form of (4) by subtraction between the fluxes

$$\begin{bmatrix}\lambda_\mathrm{a}\\ \lambda_\mathrm{b}\\ \lambda_\mathrm{c}\end{bmatrix} = \mathrm{L_{ls}}\begin{bmatrix}\mathrm{i_a}\\ \mathrm{i_b}\\ \mathrm{i_c}\end{bmatrix} + \frac{3}{2}\mathrm{L_{ms}}\begin{bmatrix}\mathrm{i_a}+\mathrm{i_r}\\ \mathrm{i_b}+\mathrm{i_s}\\ \mathrm{i_c}+\mathrm{i_t}\end{bmatrix} + \mathrm{L_{ms}T_{rs}}\begin{bmatrix}\mathrm{i_u}\\ \mathrm{i_v}\\ \mathrm{i_w}\end{bmatrix} \tag{4-a}$$

$$\begin{bmatrix}\lambda_\mathrm{r}\\ \lambda_\mathrm{s}\\ \lambda_\mathrm{t}\end{bmatrix} = \mathrm{L_{ls}}\begin{bmatrix}\mathrm{i_r}\\ \mathrm{i_s}\\ \mathrm{i_t}\end{bmatrix} + \frac{3}{2}\mathrm{L_{ms}}\begin{bmatrix}\mathrm{i_a}+\mathrm{i_r}\\ \mathrm{i_b}+\mathrm{i_s}\\ \mathrm{i_c}+\mathrm{i_t}\end{bmatrix} + \mathrm{L_{ms}T_{rs}}\begin{bmatrix}\mathrm{i_u}\\ \mathrm{i_v}\\ \mathrm{i_w}\end{bmatrix} \tag{4-b}$$

$$\begin{bmatrix}\lambda_\mathrm{u}\\ \lambda_\mathrm{v}\\ \lambda_\mathrm{w}\end{bmatrix} = \left(\mathrm{L_{lr}}+\frac{3}{2}\mathrm{L_{ms}}\right)\begin{bmatrix}\mathrm{i_u}\\ \mathrm{i_v}\\ \mathrm{i_w}\end{bmatrix} + \mathrm{L_{ms}T_{sr}}\begin{bmatrix}\mathrm{i_a}+\mathrm{i_r}\\ \mathrm{i_b}+\mathrm{i_s}\\ \mathrm{i_c}+\mathrm{i_t}\end{bmatrix} \tag{4-c}$$

$$\begin{bmatrix}\mathrm{i_u}\\ \mathrm{i_v}\\ \mathrm{i_w}\end{bmatrix} = \begin{bmatrix}\mathrm{i_{ar}}-\mathrm{i_{cr}}\\ \mathrm{i_{br}}-\mathrm{i_{ar}}\\ \mathrm{i_{cr}}-\mathrm{i_{br}}\end{bmatrix}. \tag{5}$$

A new definition of rotor currents can be derived as (5) through their subtractions to maintain the consistency between (1) and (4). That is, (4) can be regarded as a fictitious model of a DWIM as a control. In terms of converter currents, the voltage equation of a DDSW-based DWIM would be completely derived if the resistance drop is added to the time

differential of (4). Initially, the winding voltages are expressed with the converter voltages as in (6) by the superposition principle [1]

$$\begin{cases} \mathrm{v}_{\alpha 1} = \mathrm{v}_{\mathrm{ae}} - \mathrm{v}_{\mathrm{se}} \\ \mathrm{v}_{\beta 1} = \mathrm{v}_{\mathrm{be}} - \mathrm{v}_{\mathrm{te}} \\ \mathrm{v}_{\gamma 1} = \mathrm{v}_{\mathrm{ce}} - \mathrm{v}_{\mathrm{re}} \end{cases} \tag{6-a}$$

$$\begin{cases} \mathrm{v}_{\alpha 2} = \mathrm{v}_{\mathrm{re}} - \mathrm{v}_{\mathrm{be}} \\ \mathrm{v}_{\beta 2} = \mathrm{v}_{\mathrm{se}} - \mathrm{v}_{\mathrm{ce}} \\ \mathrm{v}_{\gamma 2} = \mathrm{v}_{\mathrm{te}} - \mathrm{v}_{\mathrm{ae}} \end{cases}. \tag{6-b}$$

In these equations, the subscript "e" represents the effective converter voltage without common-mode components, and the sum of the three-phase effective voltage is null. The influence of common-mode components can be disregarded for the current regulation [19].

The voltage equation can be derived with (7) through subtraction, similar to the flux in (4)

$$\begin{aligned} \begin{bmatrix} \mathrm{v}_{\mathrm{af}} \\ \mathrm{v}_{\mathrm{bf}} \\ \mathrm{v}_{\mathrm{cf}} \end{bmatrix} &= \begin{bmatrix} \mathrm{v}_{\alpha 1} - \mathrm{v}_{\gamma 2} \\ \mathrm{v}_{\beta 1} - \mathrm{v}_{\alpha 2} \\ \mathrm{v}_{\gamma 1} - \mathrm{v}_{\beta 2} \end{bmatrix} = \mathrm{R}_{\mathrm{s}} \begin{bmatrix} \mathrm{i}_{\mathrm{a}} \\ \mathrm{i}_{\mathrm{b}} \\ \mathrm{i}_{\mathrm{c}} \end{bmatrix} + \frac{d}{dt} \begin{bmatrix} \lambda_{\mathrm{a}} \\ \lambda_{\mathrm{b}} \\ \lambda_{\mathrm{c}} \end{bmatrix} \\ &= \begin{bmatrix} 2\mathrm{v}_{\mathrm{ae}} + \mathrm{v}_{\mathrm{re}} \\ 2\mathrm{v}_{\mathrm{be}} + \mathrm{v}_{\mathrm{se}} \\ 2\mathrm{v}_{\mathrm{ce}} + \mathrm{v}_{\mathrm{te}} \end{bmatrix} \end{aligned} \tag{7-a}$$

$$\begin{aligned} \begin{bmatrix} \mathrm{v}_{\mathrm{rf}} \\ \mathrm{v}_{\mathrm{sf}} \\ \mathrm{v}_{\mathrm{tf}} \end{bmatrix} &= \begin{bmatrix} \mathrm{v}_{\alpha 2} - \mathrm{v}_{\gamma 1} \\ \mathrm{v}_{\beta 2} - \mathrm{v}_{\alpha 1} \\ \mathrm{v}_{\gamma 2} - \mathrm{v}_{\beta 1} \end{bmatrix} = \mathrm{R}_{\mathrm{s}} \begin{bmatrix} \mathrm{i}_{\mathrm{r}} \\ \mathrm{i}_{\mathrm{s}} \\ \mathrm{i}_{\mathrm{t}} \end{bmatrix} + \frac{d}{dt} \begin{bmatrix} \lambda_{\mathrm{r}} \\ \lambda_{\mathrm{s}} \\ \lambda_{\mathrm{t}} \end{bmatrix} \\ &= \begin{bmatrix} 2\mathrm{v}_{\mathrm{re}} + \mathrm{v}_{\mathrm{ae}} \\ 2\mathrm{v}_{\mathrm{se}} + \mathrm{v}_{\mathrm{be}} \\ 2\mathrm{v}_{\mathrm{te}} + \mathrm{v}_{\mathrm{ce}} \end{bmatrix} \end{aligned} \tag{7-b}$$

$$\begin{bmatrix} \mathrm{v}_{\mathrm{u}} \\ \mathrm{v}_{\mathrm{v}} \\ \mathrm{v}_{\mathrm{w}} \end{bmatrix} = \begin{bmatrix} \mathrm{v}_{\mathrm{ar}} - \mathrm{v}_{\mathrm{cr}} \\ \mathrm{v}_{\mathrm{br}} - \mathrm{v}_{\mathrm{ar}} \\ \mathrm{v}_{\mathrm{cr}} - \mathrm{v}_{\mathrm{br}} \end{bmatrix} = \mathrm{R}_{\mathrm{r}} \begin{bmatrix} \mathrm{i}_{\mathrm{u}} \\ \mathrm{i}_{\mathrm{v}} \\ \mathrm{i}_{\mathrm{w}} \end{bmatrix} + \frac{d}{dt} \begin{bmatrix} \lambda_{\mathrm{u}} \\ \lambda_{\mathrm{v}} \\ \lambda_{\mathrm{w}} \end{bmatrix} \tag{7-c}$$

where $\mathrm{R_s}$ and $\mathrm{R_r}$ are the stator and rotor winding resistances, respectively.

With the concept of the complex space vector [8], the three-phase variables in (4) and (7) are presented as rotating vectors on a plane. In addition, these complex vectors can be considered in the rotating reference frame, which rotates with an arbitrary rotating frequency, ω. Then, (8) can be obtained from (4) while (9) can be determined from (7)

$$\vec{\lambda}_{\mathrm{dqs1}} = \mathrm{L_s}\vec{\mathrm{i}}_{\mathrm{dqs1}} + \mathrm{L_m}(\vec{\mathrm{i}}_{\mathrm{dqs2}} + \vec{\mathrm{i}}_{\mathrm{dqr}}) \tag{8-a}$$

$$\vec{\lambda}_{\mathrm{dqs2}} = \mathrm{L_s}\vec{\mathrm{i}}_{\mathrm{dqs2}} + \mathrm{L_m}(\vec{\mathrm{i}}_{\mathrm{dqs1}} + \vec{\mathrm{i}}_{\mathrm{dqr}}) \tag{8-b}$$

$$\vec{\lambda}_{\mathrm{dqr}} = \mathrm{L_r}\vec{\mathrm{i}}_{\mathrm{dqr}} + \mathrm{L_m}(\vec{\mathrm{i}}_{\mathrm{dqs1}} + \vec{\mathrm{i}}_{\mathrm{dqs2}}) \tag{8-c}$$

$$\vec{\mathrm{v}}_{\mathrm{dqs1}} = \mathrm{R_s}\vec{\mathrm{i}}_{\mathrm{dqs1}} + \frac{d}{dt}\vec{\lambda}_{\mathrm{dqs1}} + j\omega \cdot \vec{\lambda}_{\mathrm{dqs1}} \tag{9-a}$$

$$\vec{\mathrm{v}}_{\mathrm{dqs2}} = \mathrm{R_s}\vec{\mathrm{i}}_{\mathrm{dqs2}} + \frac{d}{dt}\vec{\lambda}_{\mathrm{dqs2}} + j\omega \cdot \vec{\lambda}_{\mathrm{dqs2}} \tag{9-b}$$

$$\vec{\mathrm{v}}_{\mathrm{dqr}} = \mathrm{R_r}\vec{\mathrm{i}}_{\mathrm{dqr}} + \frac{d}{dt}\vec{\lambda}_{\mathrm{dqr}} + j(\omega - \omega_{\mathrm{r}}) \cdot \vec{\lambda}_{\mathrm{dqr}} \tag{9-c}$$

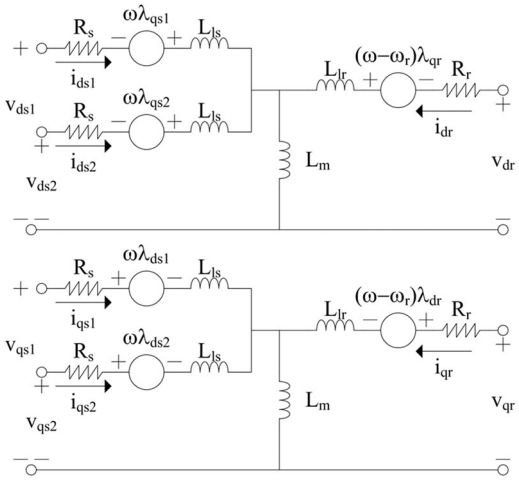

Fig. 7. Equivalent d-q model of a DDSW-applied DWIM.

where $\mathrm{L_m}$ is equal to $1.5{\cdot}L_{\mathrm{ms}}$. In addition, $\mathrm{L_s}$ is the sum of $\mathrm{L_{ls}}$ and $\mathrm{L_m}$, and $\mathrm{L_r}$ is the sum of $\mathrm{L_{lr}}$ and $\mathrm{L_m}$. To prevent confusion due to the presence of several three-phase voltages in (7), it should be noted at (9) that $\vec{\mathrm{v}}_{\mathrm{dqs1}}$ is the complex space vector from $\mathrm{v_{af}}$, $\mathrm{v_{bf}}$, and $\mathrm{v_{cf}}$ in (7). This also applies to $\vec{\mathrm{v}}_{\mathrm{dqs2}}$ from $\mathrm{v_{rf}}$, $\mathrm{v_{sf}}$, and $\mathrm{v_{tf}}$. As an example of the complex space vector, $\vec{\mathrm{v}}_{\mathrm{dqs1}}$ represents $\mathrm{v_{ds1}} + j\mathrm{v_{qs1}}$.

On the basis of (9), the equivalent circuit of the DWIM with DDSW can be depicted as shown in Fig. 7 in the arbitrary rotating reference frame, identical to those of a DWIM in the literature [11]. However, the ratings of the currents, voltages, and fluxes must be discussed further for the complete modeling of a DDSW-based DWIM.

As is well known with regard to induction machines, the d-axis rotor flux and the slip frequency are respectively derived as (10) and (11) from (9) if the synchronously rotating d-q axis is set such that the q-axis rotor flux is null. This also means that ω in (9) is set as the synchronously rotating speed

$$\lambda_{\mathrm{dr}} = \frac{\mathrm{L_m}}{1 + \mathrm{s} \cdot \mathrm{L_r}/\mathrm{R_r}}(\mathrm{i_{ds1}} + \mathrm{i_{ds2}}) \tag{10}$$

$$\omega_{\mathrm{sl}} = \omega - \omega_{\mathrm{r}} = \frac{\mathrm{R_r}}{\mathrm{L_r}}\frac{\mathrm{L_m}}{\lambda_{\mathrm{dr}}}(\mathrm{i_{qs1}} + \mathrm{i_{qs2}}) \tag{11}$$

where "s" indicates the Laplace operator.

Pertaining to the rotor flux and the slip frequency, their equations with respect to the converter current have the formats identical to those of the winding currents. However, the magnitude of the converter currents is $\sqrt{3}$ times that of the winding currents when considering (3). The rated rotor flux in the converter-based model then becomes $\sqrt{3}$ times that in the winding-based model. This has to be recognized as a scale difference between the modeling methods. As mentioned earlier, a fictitious plant was assumed to derive the flux and voltage equations in terms of the converter currents.

The scale difference also appears to arise for the slip frequency in (11) due to the q-axis currents. However, because the rotor flux in the denominator offsets the scale difference

of the q-axis currents, the magnitude of the slip frequency is identical in both of the winding-based and the converter-based models.

In addition, the torque equation can be derived from the power equation, where the products of the voltages and currents in (9) are summed. Specifically, the electrical power of the DDSW-based DWIM, $\mathrm{P_e}$, can be expressed as

$$\mathrm{P_e} = \eta_\mathrm{m} \cdot Re[\vec{\mathrm{v}}_\mathrm{dqs1} \cdot \vec{\mathrm{i}}^{*}_\mathrm{dqs1} + \vec{\mathrm{v}}_\mathrm{dqs2} \cdot \vec{\mathrm{i}}^{*}_\mathrm{dqs2} + \vec{\mathrm{v}}_\mathrm{dqr} \cdot \vec{\mathrm{i}}^{*}_\mathrm{dqr}] \quad (12)$$

where the asterisk "$*$" represents the complex conjugate, and η_m is introduced for scaling.

After eliminating copper losses and the varying energy of the inductances [8], the component related to the torque can be separated. Thus, the torque equation can be derived as

$$\mathrm{T_e} = \frac{1}{2}\frac{\mathrm{P}}{2}\frac{\mathrm{L_m}}{\mathrm{L_r}} \cdot \lambda_\mathrm{dr}(\mathrm{i_{qs1}} + \mathrm{i_{qs2}}). \quad (13)$$

Because the rotor flux and the q-axis current in the converter-based model are $\sqrt{3}$ times their counterparts in the winding-based model, η_m must be 1/2 for a consistent power dimension.

As is widely known in the literature [8], vector control for a DDSW-based DWIM can also be achieved by adjusting the d-q currents when considering (10) and (13). Specifically, the d-axis currents are effective when used to modulate the rotor flux, while the q-axis currents can be used to modulate the torque. In addition, the synchronous frequency can be obtained from the sum of the slip frequency from (11) and the rotating frequency ω_r.

IV. Decoupling Method for Current Regulation

Regulation of the converter currents is essential because the torque and flux are modulated by regulating these currents. However, this regulation is not simple because multiple couplings between the converters exist in terms of the voltage and current.

Initially, voltage coupling should be considered, which can be understood with (7). In the equation, each converter current is affected by two effective voltages, denoted by the subscript "e," from different converters. That is, current regulation of one converter cannot be achieved without considering the output of the other converter. This fact is confusing when designing the current regulation because six phases appear to be considered together.

This voltage coupling problem can be solved by adding an intermediate stage. According to (7), the "abc" current is only affected by $\mathrm{v_{af}}$, $\mathrm{v_{bf}}$, and $\mathrm{v_{cf}}$, while the "rst" current is affected by $\mathrm{v_{rf}}$, $\mathrm{v_{sf}}$, and $\mathrm{v_{tf}}$. That is, in terms of these intermediate voltages, current regulators can be separately designed as if each converter is operating independently. After the regulators compute the references into intermediate voltages, they can be translated into the actual voltage references for each converter. This translation can be derived from (7) as (14) in the d-q reference frame

$$\mathrm{T_P} = \frac{2}{3}\begin{bmatrix} \cos\theta_\mathrm{r} & \cos\left(\theta_\mathrm{r} - \frac{2\pi}{3}\right) & \cos\left(\theta_\mathrm{r} + \frac{2\pi}{3}\right) \\ -\sin\theta_\mathrm{r} & -\sin\left(\theta_\mathrm{r} - \frac{2\pi}{3}\right) & -\sin\left(\theta_\mathrm{r} + \frac{2\pi}{3}\right) \end{bmatrix} \quad (14\text{-a})$$

$$\begin{bmatrix} \mathrm{v_{ds1}} \\ \mathrm{v_{qs1}} \end{bmatrix} = \mathrm{T_P}\begin{bmatrix} \mathrm{v_{af}} \\ \mathrm{v_{bf}} \\ \mathrm{v_{cf}} \end{bmatrix} = \mathrm{T_P}\begin{bmatrix} 2\mathrm{v_{ae}} + \mathrm{v_{re}} \\ 2\mathrm{v_{be}} + \mathrm{v_{se}} \\ 2\mathrm{v_{ce}} + \mathrm{v_{te}} \end{bmatrix} = \begin{bmatrix} 2\mathrm{v_{d1}} + \mathrm{v_{d2}} \\ 2\mathrm{v_{q1}} + \mathrm{v_{q2}} \end{bmatrix} \quad (14\text{-b})$$

$$\begin{bmatrix} \mathrm{v_{ds2}} \\ \mathrm{v_{qs2}} \end{bmatrix} = \mathrm{T_P}\begin{bmatrix} \mathrm{v_{rf}} \\ \mathrm{v_{sf}} \\ \mathrm{v_{tf}} \end{bmatrix} = \mathrm{T_P}\begin{bmatrix} 2\mathrm{v_{re}} + \mathrm{v_{ae}} \\ 2\mathrm{v_{se}} + \mathrm{v_{be}} \\ 2\mathrm{v_{te}} + \mathrm{v_{ce}} \end{bmatrix} = \begin{bmatrix} \mathrm{v_{d1}} + 2\mathrm{v_{d2}} \\ \mathrm{v_{q1}} + 2\mathrm{v_{q2}} \end{bmatrix} \quad (14\text{-c})$$

$$\begin{bmatrix} \mathrm{v_{d1}} \\ \mathrm{v_{d2}} \\ \mathrm{v_{q1}} \\ \mathrm{v_{q2}} \end{bmatrix} = \frac{1}{3}\begin{bmatrix} 2 & -1 & 0 & 0 \\ -1 & 2 & 0 & 0 \\ 0 & 0 & 2 & -1 \\ 0 & 0 & -1 & 2 \end{bmatrix}\begin{bmatrix} \mathrm{v_{ds1}} \\ \mathrm{v_{ds2}} \\ \mathrm{v_{qs1}} \\ \mathrm{v_{qs2}} \end{bmatrix} \quad (14\text{-d})$$

where $\mathrm{v_{d1}}$, $\mathrm{v_{q1}}$, $\mathrm{v_{d2}}$, and $\mathrm{v_{q2}}$ are the d-q voltages of the effective converter voltages, while $\mathrm{v_{ds1}}$, $\mathrm{v_{qs1}}$, $\mathrm{v_{ds2}}$, and $\mathrm{v_{qs2}}$ are those of the intermediate voltages.

At this stage, the current coupling should be considered as well, as defined by (4). In a manner similar to voltage coupling, each instance of stator flux is affected by two currents from different converters. When considering (8) and (9), this current coupling results in flux coupling.

In order to discuss flux decoupling, the voltage equation needs to be changed from (9) to (15) by eliminating the rotor current variables, which are not deemed measurable variables in squirrel-cage induction machines [12]

$$\begin{aligned} \vec{\mathrm{v}}_\mathrm{dqs1} = {} & \left(\mathrm{R_s} + \frac{\mathrm{R_r}\mathrm{L_m^2}}{\mathrm{L_r^2}}\right)\vec{\mathrm{i}}_\mathrm{dqs1} + \mathrm{L_{ss}}\frac{d}{dt}\vec{\mathrm{i}}_\mathrm{dqs1} + \mathrm{L_{sc}}\frac{d}{dt}\vec{\mathrm{i}}_\mathrm{dqs2} \\ & + \frac{\mathrm{R_r}\mathrm{L_m^2}}{\mathrm{L_r^2}}\vec{\mathrm{i}}_\mathrm{dqs2} + j\omega\mathrm{L_{ls}}\vec{\mathrm{i}}_\mathrm{dqs1} + \vec{\mathrm{v}}_\mathrm{comm} \end{aligned} \quad (15\text{-a})$$

$$\begin{aligned} \vec{\mathrm{v}}_\mathrm{dqs2} = {} & \left(\mathrm{R_s} + \frac{\mathrm{R_r}\mathrm{L_m^2}}{\mathrm{L_r^2}}\right)\vec{\mathrm{i}}_\mathrm{dqs2} + \mathrm{L_{ss}}\frac{d}{dt}\vec{\mathrm{i}}_\mathrm{dqs2} + \mathrm{L_{sc}}\frac{d}{dt}\vec{\mathrm{i}}_\mathrm{dqs1} \\ & + \frac{\mathrm{R_r}\mathrm{L_m^2}}{\mathrm{L_r^2}}\vec{\mathrm{i}}_\mathrm{dqs1} + j\omega\mathrm{L_{ls}}\vec{\mathrm{i}}_\mathrm{dqs2} + \vec{\mathrm{v}}_\mathrm{comm} \end{aligned} \quad (15\text{-b})$$

$$\mathrm{L_{sc}} = \mathrm{L_m} - \mathrm{L_m^2}/\mathrm{L_r} \quad (15\text{-c})$$

$$\mathrm{L_{ss}} = \mathrm{L_s} - \mathrm{L_m^2}/\mathrm{L_r} = \mathrm{L_{ls}} + \mathrm{L_{sc}} \quad (15\text{-d})$$

$$\vec{\mathrm{v}}_\mathrm{comm} = \frac{\mathrm{L_m}}{\mathrm{L_r}}\left(-\frac{\mathrm{R_r}}{\mathrm{L_r}} + j\omega_\mathrm{r}\right) \cdot \vec{\lambda}_\mathrm{dqr} + j\omega\mathrm{L_{sc}}(\vec{\mathrm{i}}_\mathrm{dqs1} + \vec{\mathrm{i}}_\mathrm{dqs2}). \quad (15\text{-e})$$

Due to the flux coupling, there are cross-coupled differential terms in (15-a) and (15-b). In the literature, this differential cross-coupling is ignored, and only speed-related terms are used for feed-forward control in addition to the output of the proportional and integral (PI) controllers [12]. For flux decoupling

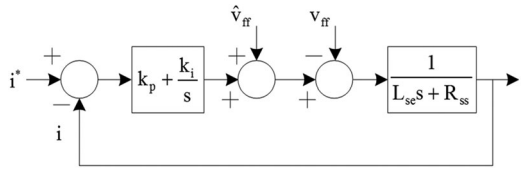

Fig. 8. Fundamental structure of a current regulator.

control, (15) can be rearranged again into

$$\begin{bmatrix} L_{ss} & L_{sc} \\ L_{sc} & L_{ss} \end{bmatrix} \cdot \frac{d}{dt} \begin{bmatrix} \vec{i}_{dqs1} \\ \vec{i}_{dqs2} \end{bmatrix} = \begin{bmatrix} \vec{v}_{dqs1} \\ \vec{v}_{dqs2} \end{bmatrix} - \begin{bmatrix} \left(R_s + \frac{R_r L_m^2}{L_r^2}\right)\vec{i}_{dqs1} + \frac{R_r L_m^2}{L_r^2}\vec{i}_{dqs2} + j\omega L_{ls}\vec{i}_{dqs1} + \vec{v}_{comm} \\ \left(R_s + \frac{R_r L_m^2}{L_r^2}\right)\vec{i}_{dqs2} + \frac{R_r L_m^2}{L_r^2}\vec{i}_{dqs1} + j\omega L_{ls}\vec{i}_{dqs2} + \vec{v}_{comm} \end{bmatrix} \cdot \tag{16}$$

Then, the voltage equation can be derived as (17) through matrix inversion

$$\begin{bmatrix} \vec{v}_{dqe1} \\ \vec{v}_{dqe2} \end{bmatrix} = R_{ss} \begin{bmatrix} \vec{i}_{dqs1} \\ \vec{i}_{dqs2} \end{bmatrix} + L_{se} \frac{d}{dt} \begin{bmatrix} \vec{i}_{dqs1} \\ \vec{i}_{dqs2} \end{bmatrix} + \begin{bmatrix} R_{sc}\vec{i}_{dqs2} + j\omega(L_{ss}\vec{i}_{dqs1} - L_{sc}\vec{i}_{dqs2}) + \vec{v}_{comm} \\ R_{sc}\vec{i}_{dqs1} + j\omega(L_{ss}\vec{i}_{dqs2} - L_{sc}\vec{i}_{dqs1}) + \vec{v}_{comm} \end{bmatrix} \tag{17-a}$$

$$\begin{bmatrix} \vec{v}_{dqs1} \\ \vec{v}_{dqs2} \end{bmatrix} = \frac{1}{L_{se}} \begin{bmatrix} L_{ss} & L_{sc} \\ L_{sc} & L_{ss} \end{bmatrix} \begin{bmatrix} \vec{v}_{dqe1} \\ \vec{v}_{dqe2} \end{bmatrix} \tag{17-b}$$

$$R_{ss} = \frac{R_s L_{ss}}{L_{ls}} + \frac{R_r L_m^2}{L_r^2} \tag{17-c}$$

$$R_{sc} = \frac{R_r L_m^2}{L_r^2} - \frac{R_s L_{sc}}{L_{ls}} \tag{17-d}$$

$$L_{se} = L_{ss} + L_{sc}. \tag{17-e}$$

Here, the differential cross coupling shown in (15) no longer appears in (17) by virtue of the matrix inversion of (16). However, the transformation of the voltage references in (17-b) is also required for this decoupling effect. The current regulators can then be designed with respect to (17-a) instead of (15).

The electrical circuit of every axis in (17-a) can be modeled with an $R_{ss} - L_{se}$ load and another disturbance that is described by the third term on the right side in the equation. Then, when a PI controller is employed, the control block diagram for each axis is drawn as shown in Fig. 8. In order to compensate for the disturbance in (17-a), which is also denoted by v_{ff} in Fig. 8, its estimated form, $\hat{v}_{ff}$, can be fed-forward. If this feed-forward compensation is perfect ($\hat{v}_{ff} = v_{ff}$), the dynamic response of the current regulation can be expressed as (18) by setting the PI gains according to (19) [20]

$$\frac{i}{i^*} = \frac{\omega_c}{s + \omega_c} \tag{18}$$

$$k_p = L_{se}\omega_c,\ k_i = R_{ss}\omega_c \tag{19}$$

where ω_c is the bandwidth of the current regulator. That is, if the parameters are accurate in terms of the gain setting and the feed-forward compensation, the response of the current regulation would be that of a first-order low-pass filter.

V. Single-Converter Operation in a DDSW-Based DWIM

Two converters are fundamental for DDSW, as shown in Fig. 1. However, one of them can be dropped out for any reason, such as a fault. In preparation for such a disconnection, single-converter operation needs to be considered. For instance, if the "rst" converter is disconnected in Fig. 1, the voltage equation can be derived via (20) due to the series connection of each winding

$$\begin{bmatrix} 3v_{ae} \\ 3v_{be} \\ 3v_{ce} \end{bmatrix} = 2R_s \begin{bmatrix} i_a \\ i_b \\ i_c \end{bmatrix} + \frac{d}{dt} \begin{bmatrix} \lambda_{\alpha 1} + \lambda_{\beta 2} - \lambda_{\beta 1} - \lambda_{\gamma 2} \\ \lambda_{\beta 1} + \lambda_{\gamma 2} - \lambda_{\gamma 1} - \lambda_{\alpha 2} \\ \lambda_{\gamma 1} + \lambda_{\alpha 2} - \lambda_{\alpha 1} - \lambda_{\beta 2} \end{bmatrix} = 2R_s \begin{bmatrix} i_a \\ i_b \\ i_c \end{bmatrix} + \frac{d}{dt} \begin{bmatrix} \lambda_a \\ \lambda_b \\ \lambda_c \end{bmatrix}. \tag{20}$$

In fact, the "abc" flux in (20) differs from that in (4), and it can be defined as

$$\begin{bmatrix} \lambda_a \\ \lambda_b \\ \lambda_c \end{bmatrix} = \left(2L_{ls} + \frac{3}{2}L_{ms}\right) \begin{bmatrix} i_a \\ i_b \\ i_c \end{bmatrix} + L_{ms} T_{rsf} \begin{bmatrix} i_x \\ i_y \\ i_z \end{bmatrix} \tag{21-a}$$

$$\begin{bmatrix} i_x \\ i_y \\ i_z \end{bmatrix} = \begin{bmatrix} i_{ar} - i_{br} \\ i_{br} - i_{cr} \\ i_{cr} - i_{ar} \end{bmatrix} \tag{21-b}$$

$$T_{rsf} = \begin{bmatrix} \cos\left(\theta_r - \frac{\pi}{3}\right) & \cos\left(\theta_r + \frac{\pi}{3}\right) & \cos(\theta_r + \pi) \\ \cos(\theta_r + \pi) & \cos\left(\theta_r - \frac{\pi}{3}\right) & \cos\left(\theta_r + \frac{\pi}{3}\right) \\ \cos\left(\theta_r + \frac{\pi}{3}\right) & \cos(\theta_r + \pi) & \cos\left(\theta_r - \frac{\pi}{3}\right) \end{bmatrix} \tag{21-c}$$

Moreover, given that the subtractions between the rotor currents in (21-b) are also different from those in (5), the rotor flux equation is newly derived as

$$\begin{bmatrix} \lambda_x \\ \lambda_y \\ \lambda_z \end{bmatrix} = \begin{bmatrix} \lambda_{ar} - \lambda_{br} \\ \lambda_{br} - \lambda_{cr} \\ \lambda_{cr} - \lambda_{ar} \end{bmatrix} = \left(L_{lr} + \frac{3}{2}L_{ms}\right) \begin{bmatrix} i_x \\ i_y \\ i_z \end{bmatrix} + L_{ms} T_{srf} \begin{bmatrix} i_a \\ i_b \\ i_c \end{bmatrix} \tag{22-a}$$

$$T_{srf}[\theta_r] = \begin{bmatrix} \cos\left(\theta_r - \frac{\pi}{3}\right) & \cos(\theta_r + \pi) & \cos\left(\theta_r + \frac{\pi}{3}\right) \\ \cos\left(\theta_r + \frac{\pi}{3}\right) & \cos\left(\theta_r - \frac{\pi}{3}\right) & \cos(\theta_r + \pi) \\ \cos(\theta_r + \pi) & \cos\left(\theta_r + \frac{\pi}{3}\right) & \cos\left(\theta_r - \frac{\pi}{3}\right) \end{bmatrix}. \tag{22-b}$$

Through similar derivations, the rotor flux and the slip frequency can be represented as

$$\lambda_{dr} = \frac{L_m}{1 + s \cdot L_r/R_r} i_{ds1} \tag{23}$$

$$\omega_{sl} = \omega - \omega_r = \frac{R_r}{L_r}\frac{L_m}{\lambda_{dr}} i_{qs1}. \tag{24}$$

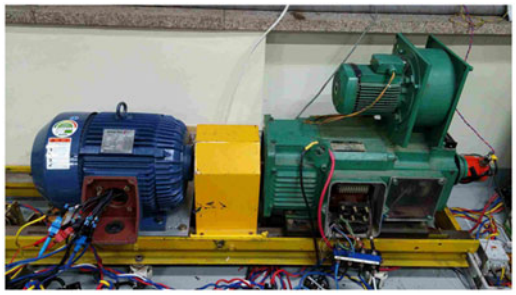

Fig. 9. Test machine (left) and load machine (right).

Fig. 10. Two converters connected to the test machine.

When compared to (10) and (11), the currents related to the "rst" converter are disappeared in (23) and (24). This feature is also observed in the torque equation under the single-converter operation

$$\mathrm{T_e} = \frac{1}{2} \cdot \frac{\mathrm{P}}{2} \frac{\mathrm{L_m}}{\mathrm{L_r}} \cdot \lambda_{\mathrm{dr}} \cdot \mathrm{i_{qs1}}. \tag{25}$$

That is, if identical currents are kept on the d-q axis of the remaining converter, the torque output during the single-converter operation becomes one quarter that under normal operation. However, because the rated excitation current, referring to the rated d-axis current, is less than one quarter of the rated winding current in large-scale induction machines, the d-axis current under the single-converter operation can be increased further. That is, even if the d-axis current is doubled for the remaining converter, the maximum q-axis current is not significantly reduced for the purpose of limiting the current. By doubling the d-axis current under the single-converter operation, the torque and the output power can be extended to nearly half of their rated counterparts under normal operation. For the current regulation, the voltage equation in (26) is finally derived. Because there is no cross coupling during the single-converter operation, the current regulators can be simply designed according to (26) in the manner displayed in (17-a) and in Fig. 8

$$\begin{aligned} 3\vec{\mathrm{v}}_{\mathrm{dq}} = \; & 2\Big(\mathrm{R_s} + \frac{\mathrm{R_r L_m^2}}{\mathrm{L_r^2}}\Big)\vec{\mathrm{i}}_{\mathrm{dqs}} + \mathrm{L_{sf}} \frac{d}{dt}\vec{\mathrm{i}}_{\mathrm{dqs}} \\ & + \frac{\mathrm{L_m}}{\mathrm{L_r}}\Big(- \frac{2\mathrm{R_r}}{\mathrm{L_r}} + j\omega_{\mathrm{r}}\Big) \cdot \vec{\lambda}_{\mathrm{dqr}} + j\omega \mathrm{L_{sf}} \vec{\mathrm{i}}_{\mathrm{dqs}} \quad \text{(26-a)} \\ \mathrm{L_{sf}} = \; & \mathrm{L_{ss}} + \mathrm{L_{ls}}. \quad \text{(26-b)} \end{aligned}$$

VI. Experimental Results

An 11-kW (1800 r/min, 58 N·m) DWIM, as shown in Fig. 9, with a voltage rating of 220/440 V, is used in the discussion of the proposed modeling and control methods for a DDSW-based DWIM. According to the definitions in (8) and (9), $\mathrm{R_s}$ and $\mathrm{R_r}$ were 0.478 and 0.172 Ω, while $\mathrm{L_{ls}}(\approx \mathrm{L_{lr}})$ and $\mathrm{L_m}$ were 1.449 and 55.54 mH, respectively. A dc machine was mechanically coupled with DWIM to generate various load conditions. In addition, two-level converters were composed of 600-V 75-A intelligent power modules, as shown in Fig. 10, and their dc links were set to 310 V. The carrier frequency was set to 2.5 kHz for the subsequent experiments, while the results shown in Figs. 2–5 were obtained with 1.25 kHz carriers to show more obvious differences. The carrier frequency was set low enough to emulate multimegawatt drives. All of the control algorithms were digitally implemented in a DSP board based on TMS320C28346.

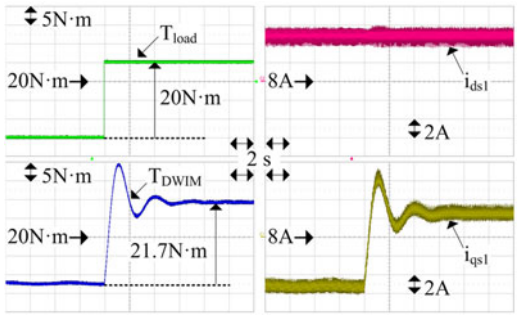

Fig. 11. Torque output under normal operation.

Initially, the torque equation in (13) was examined as shown in Fig. 11, where the test machine was under a speed control scheme at 1200 r/min, and the load torque, $\mathrm{T_{load}}$, was changed by 20 N·m. Although the torque output of the test machine, $\mathrm{T_{DWIM}}$, was changed by 21.7 N·m, it should be noted that $\mathrm{T_{DWIM}}$ and $\mathrm{T_{load}}$ in Fig. 11 were calculated with each machine's parameters. Although the parameter estimations were carried out to be as accurate as possible, some parameter errors may be reflected. During several tests with different torque variations, only negligible errors between $\mathrm{T_{DWIM}}$ and $\mathrm{T_{load}}$ were observed. Therefore, it is confirmed that the value of 1/2 is appropriate for η_{m} in (12). In Fig. 11, the d-q current is presented only for the "abc" converter because it was nearly identical to that of the "rst" converter.

The majority of high-power motor drives are related to fan/pump operations, where the load is proportional to the square of the rotation speed. Thus, the fan/pump load was emulated using the load machine, as shown in Figs. 12 and 13. Because the d-axis currents are constantly regulated to their rated value in Fig. 13, the q-axis currents are similarly changed with $\mathrm{T_{load}}$ in Fig. 12. The aspect of the ripple currents in Fig. 13 was changed because the PWM property of DDSW varied depending on the modulation index.

To discuss the decoupling method, the load machine was speed controlled at 900 r/min, while the test machine was torque controlled. Then, $\mathrm{T_{DWIM}}$ was step changed by 30 N·m, as

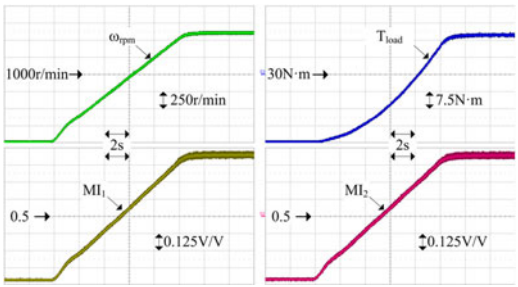

Fig. 12. Fan/pump emulation—speed, torque, and modulation indices.

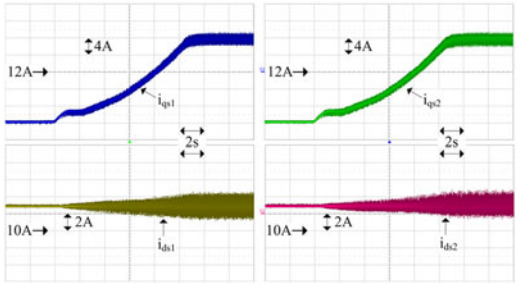

Fig. 13. Fan/pump emulation—d-q currents.

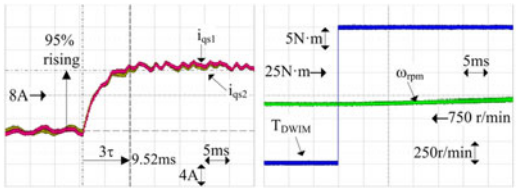

Fig. 14. Dynamics of the current regulation—conventional method.

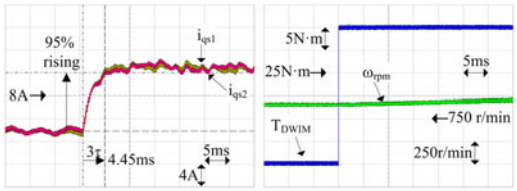

Fig. 15. Dynamics of the current regulation—proposed method.

shown in Figs. 14 and 15, where the decoupling methods were different. Because the current responses to their references were designed to follow (18), those responses could be numerically described with their bandwidth. Specifically, when the intended bandwidth was 150 Hz in all cases when using the same parameters for each gain setting, the actual bandwidth was computed as 50.2 Hz from 3τ in Fig. 14 for the conventional method [12], whereas it was 107.3 Hz in Fig. 15 for the proposed decoupling method. This improvement was possible because the cross-coupled differential terms were successfully decoupled in the proposed method. Although the bandwidth of the proposed method remained smaller than the designed bandwidth,

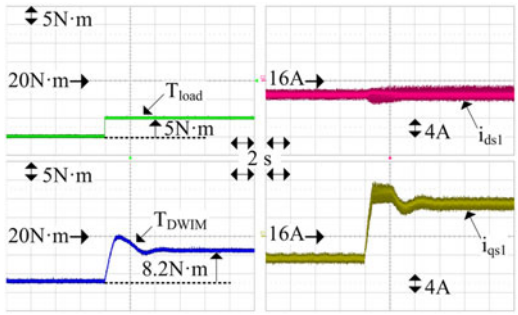

Fig. 16. Torque output under single-converter operation.

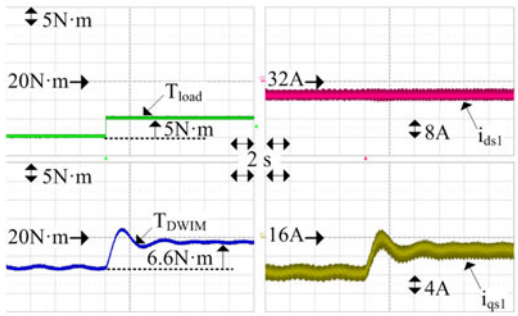

Fig. 17. Torque output under single-converter operation at twice the d-axis current.

it should be noted that nominal parameters were used for the gain settings, and the feed-forward compensation scheme may not be perfect.

In addition, the torque equation of (25) was examined under single-converter operation, where the "rst" converter is disconnected. As a reduction of the torque per current was expected, the load torque was changed by 5 N·m at 1200 r/min, as shown in Fig. 16, which was one quarter of that in Fig. 11. The q-axis current was then changed by 11.7 A to increase 8.2 N·m in T_{DWIM}. In other words, the torque per q-axis current was 0.7 N·m/A, whereas it is 1.36 N·m/A in Fig. 11. This occurs because the rotor flux was halved during the single-converter operation. In Fig. 17, the results when doubling the d-axis current are shown against identical load torque variations. The torque per q-axis current in the figure became twice that in Fig. 16. That is, during the single-converter operation, if the rotor flux is maintained as the original rated value of the normal operation, the torque capability can be held at half that during the normal operation.

To show ripple currents during the single-converter operation, the converter currents are shown in Fig. 18 at the rated speed with no load torque. In addition, the carrier frequency was set to 1.25 kHz for a fair comparison to the results shown in Figs. 4 and 5. In principle, it appears plausible that the ripple property worsens under the single-converter operation because one of the converters is dropped out during the interleaving process. However, as shown in Fig. 18, the THD of i_a was 11.2% when the fundamental current was 13.5 A. That is, the harmonic property

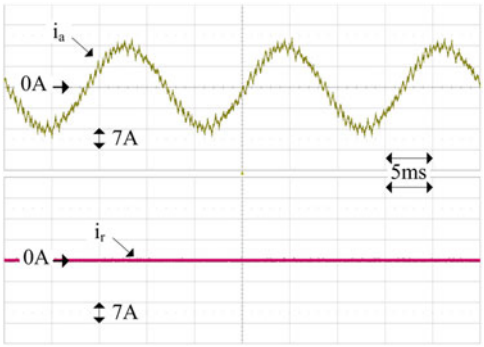

Fig. 18. Converter currents under fault operation.

under single-converter operation is comparable to that under normal DDSW operation. A more detailed description of this phenomenon is available in the literature [19]. That is, even if the turn number of windings is doubled by the series connections in the single-converter operation, the magnitude of stator fluxes is not doubled as shown in (20). This is why the maximum power becomes halved in the single-converter operation. Although the utilization factor of the windings is normally desirable to be large in the view point of power conversion, its reduction is inevitable under the single-converter operation. However, these surplus windings can contribute to the interleaving effect shown in Fig. 18 because two different-phase windings are excited by one line-to-line voltage that is pulse-width modulated by the single converter.

VII. Conclusion

In this paper, the application of DDSW to a DWIM was discussed. Initially, it was described how vector control is implemented for a DDSW-based DWIM. For control purposes, an equivalent model was derived with respect to the converter currents. The feasibility of the proposed vector control scheme was tested by emulating a fan/pump load. In addition, a decoupling method between the converters was proposed to improve the dynamic response of the current regulation. As a result, the control bandwidth could be increased by 113.7% when identical parameters were used for control settings. Finally, the single-converter operation was also considered, where one of the converters is disconnected from DDSW. For this operation, after vector control was discussed, the ripple properties were shown in terms of the converter current. It was confirmed that the torque capability under single-converter operation can be held to half that under normal operation without any degradation of the ripple of the converter current. This paper has been previously presented in the conference [21].

References

[1] Y. Park, S. Ohn, and S.-K. Sul, "Multi-level operation with two-level converters through a double-delta source connected transformer," *J. Power Electron.*, vol. 14, no. 6, pp. 1093–1099, Nov. 2014.

[2] S. Brisset, D. Vizireanu, and P. Brochet, "Design and optimization of a nine-phase axial-flux PM synchronous generator with concentrated winding for direct-drive wind turbine," *IEEE Trans. Ind. Appl.*, vol. 44, no. 3, pp. 707–715, May/Jun. 2008.

[3] F. B. Grigoletto and H. Pinheiro, "Flexible arrangement of static converters for grid-connected wind energy conversion systems," *IEEE Trans. Ind. Electron.*, vol. 61, no. 9, pp. 4707–4721, Sep. 2014.

[4] E. Cengelci, P. N. Enjeti, and J. W. Gray, "A new modular motor-modular inverter concept for medium-voltage adjustable-speed-drive systems," *IEEE Trans. Ind. Appl.*, vol. 36, no. 3, pp. 786–796, May/Jun. 2000.

[5] S. Malik and D. Kluge, "ACS1000 world's first standard AC drive for medium-voltage applications," *ABB Rev.*, no. 2, pp. 4–11, 1998.

[6] P. Vas, "Induction machine windings, starting, braking, and speed control techniques," in *Electrical Machines and Drives a Space-Vector Theory Approach*. New York, NY, USA: Oxford Univ. Press, 1992, ch. 3.1, pp. 224–225.

[7] A. L. Sheldrake, "Methods of starting induction motors," in *Handbook of Electrical Engineering for Practitioners in the Oil, Gas, and Petrochemical Industry*. Hoboken, NJ, USA: Wiley, 2003, ch. 5.10, pp. 125–129.

[8] D. W. Novotny and T. A. Lipo, "d, q modeling of induction and synchronous machines," in *Vector Control and Dynamics of AC Drives*. New York, NY, USA: Oxford Univ. Press, 1996, ch. 2, pp. 35–107.

[9] Z. Qu, M. Ranta, M. Hinkkanen, and J. Luomi, "Loss-minimizing flux level control of induction motor drives," *IEEE Trans. Ind. Appl*., vol. 48, no. 3, pp. 952–961, May/Jun. 2012.

[10] G. Pellegrino, R. I. Bojoi, and P. Guglielmi, "Unified direct-flux vector control for AC motor drives," *IEEE Trans. Ind. Appl.*, vol. 47, no. 5, pp. 2093–2102, Sep./Oct. 2011.

[11] R. H. Nelson and P. C. Krause, "Induction machine analysis for arbitrary displacement between multiple winding sets," *IEEE Trans. Power App. Syst.*, vol. PAS-93, no. 3, pp. 841–848, May 1974.

[12] R. Bojoi, F. Profumo, and A. Tenconi, "Digital synchronous frame current regulation for dual three-phase induction motor drives," in *Proc. IEEE Power Electron. Spec. Conf.*, Jun. 15–19, 2003, vol. 3, pp. 1475–1480.

[13] S. Schroder *et al.*, "Modular high-power shunt-interleaved drive system: A realization up to 35 MW for oil and gas applications," *IEEE Trans. Ind. Appl.*, vol. 46, no. 2, pp. 821–830, Mar./Apr. 2010.

[14] A. R. Munoz and T. A. Lipo, "Dual-stator winding induction machine drive," *IEEE Trans. Ind. Appl.*, vol. 36, no. 5, pp. 1369–1379, Sep./Oct. 2000.

[15] T. Geyer and S. Schroder, "Reliability considerations and fault-handling strategies for multi-MW modular drive systems," *IEEE Trans. Ind. Appl.*, vol. 46, no. 6, pp. 2442–2451, Nov./Dec. 2010.

[16] H. Zhong, L. Zhao, and X. Li, "Design and analysis of a three-phase rotary transformer for doubly fed induction generators," *IEEE Trans. Ind. Appl.*, vol. 51, no. 4, pp. 2791–2796, Jul./Aug. 2015.

[17] T. A. Lipo, "A d-q Model for six phase induction machines," in *Proc. Int. Conf. Electr. Mach.*, 1980, pp. 860–867.

[18] O. Ojo and I. E. Davidson, "PWM-VSI inverter-assisted stand-alone dual-stator winding induction generator," *IEEE Trans. Ind. Appl.*, vol. 36, no. 6, pp. 1604–1611, Nov./Dec. 2000.

[19] Y. Park, J.-M. Yoo, and S.-K. Sul, "Current regulation and fault tolerance in double-delta sourced transformer," in *Proc. 2015 IEEE Energy Convers. Congr. Expo.*, Montreal, QC, Canada, 2015, pp. 1541–1548.

[20] S.-K. Sul, "Design of regulators for electric machines and power converters," in *Control of Electric Machine Drive Systems*. Hoboken, NJ, USA: Wiley, 2011, ch. 4, pp. 154–282.

[21] Y. Park, J.-M. Yoo, and S.-K. Sul, "Double-delta sourced winding for dual-winding induction machine," in *Proc. 2015 9th Int. Conf. Power Electron. ECCE Asia*, Jun. 1–5, 2015, pp. 77–85.

Yongsoon Park (S'12–M'15) received the B.S., M.S., and Ph.D. degrees in electrical engineering from Seoul National University, Seoul, South Korea, in 2008, 2010, and 2015, respectively.

From 2015 to 2016, he was a Senior Engineer with Samsung Electronics, Co., Ltd., South Korea. Since 2016, he has been with the Gwangju Institute of Science and Technology, Gwangju, South Korea, where he is currently an Assistant Professor. His current research interests include design and control of power conversion circuits for grid connection and motor drives.

Jeong-Mock Yoo was born in South Korea in 1991. He received the B.S. and M.S. degrees in electrical engineering from Seoul National University, Seoul, South Korea, in 2014 and 2016, respectively.

He is currently a Research Engineer with the Yura Corporation R&D Center, Pangyo, Seongnam-si, South Korea. His research interests include power electronics and design and control of power converters for automotive application.

Seung-Ki Sul (S'78–M'87–SM'98–F'00) received the B.S., M.S., and Ph.D. degrees in electrical engineering from Seoul National University, Seoul, South Korea, in 1980, 1983, and 1986, respectively.

From 1986 to 1988, he was an Associate Researcher in the Department of Electrical and Computer Engineering, University of Wisconsin, Madison, USA. From 1988 to 1990, he was a Principal Research Engineer with LG Industrial Systems Company, South Korea. For a year of 2015, he served as the President of Korea Institute of Power Electronics, Seoul. Since 1991, he has been a Member of the Faculty with the School of the Electrical and Computer Engineering, Seoul National University, where he is currently a Professor. He published more than 140 IEEE reviewed journal papers and a total of more than 330 international conference papers in the area of power electronics. He holds 14 U.S. patents, seven Japanese patents, 11 Korean patents, and granted 38 Ph.D.s under his supervision. His current research interests include control of electrical machines, electric/hybrid vehicles, electric propulsion of ship, and power conditioning system for renewables.

Dr. Sul received many best paper awards from international conferences and journals including the first and second best paper awards, simultaneously from the IEEE TRANSACTIONS ON INDUSTRY APPLICATIONS in 2015. He also received the IEEE IAS Outstanding Achievement Award in 2016. He was the Program Chair of the IEEE PESC'06 and a General Chair of the IEEE ECCE-Asia, ICPE, 2011.